PCCP

Accepted Manuscript

ROYAL SOCIETY OF CHEMISTRY

www.rsc.org/pccp

Trends in non-metal doping of $SrTiO_3$ surface: a hybrid density functional study

Yating Guo [a], Xiaowei Qiu [a], Hao Dong [a,*] , Xin Zhou [b,*]

[a] Institute of Chemistry for Functionalized Materials, School of Chemistry and Chemical Engineering, Liaoning Normal University, Dalian, Liaoning 116029, China

[b] State Key Laboratory of Catalysis, Dalian Institute of Chemical Physics, Chinese Academy of Sciences, Dalian National Laboratory for Clean Energy, Dalian, Liaoning 116023, China

* Corresponding author.

E-mail addresses: sinodonghao@gmail.com (H. Dong) xzhou@dicp.ac.cn (X. Zhou)

Abstract

$SrTiO_3$ surface doping with non-metal atoms (X=C, N, F, Si, P, S, Cl, Se, Br and I) has been considered in a systematic study by performing periodic density functional theory calculations with the hybrid HSE06 functional, with the objective of improving its photocatalytic activity for water splitting under visible light. Our results find that the doping in the top layer of $SrTiO_3$ (001) surface is energetically favored. X (X=C, N and F) atom with relatively smaller atom radius tends to substitute the O atom in the TiO_2-terminated surface while the preferential occupation of the X(X=P, S, Cl, Se and Br) atom with larger atom radius takes place at the O position in the SrO-terminated surface. X-doped surfaces (X=C, Si and P) show the presence of discrete midgap states, which are detrimental for photocatalysis. Due to the appearance of surface O 2p states, the band gap of pure TiO_2-terminated surface is calculated to be 2.56 eV, which is much narrower than that of bulk $SrTiO_3$ (3.4 eV). Our results indicate that the band alignments of N-doped, Br-doped and I-doped $SrTiO_3$ (001) surfaces are well positioned for the feasibility of photo-oxidation and photo-reduction of water, which are promising for water splitting in the visible light region.

1. Introduction

Photocatalytic splitting of water into hydrogen and oxygen using a heterogeneous photocatalyst is a potentially clean and renewable solution to convert solar energy into hydrogen fuel. [1-6] In this field, one of the most important issues is the development of suitable semiconductors as photocatalytsts. Among the vast majority of the active photocatalysts for water splitting, layer structured perovskite titanates are considered as one of the ideal building blocks for the assembly of a water splitting photocatalysts. [7-11] Perovskite titanates are n-type semiconductors constituted of earth abundant elements, and usually are stable in aqueous solutions. Unfortunately, due to the large band gaps (>3.0 eV), their practical applications have been restricted to the ultraviolet region, which only occupies about 5% of the whole solar radiation spectrum. Among many methods developed to extend the light absorption of photocatalysts into the visible region,[12-16] doping foreign elements into a semiconductor has been proved to be an effective strategy.

$SrTiO_3$ as a representative of prominent perovskite titanates has been already doped with different non-metal dopants for visible-light absorption.[17-24] Wang *et al.* applied mechanochemical reaction to perform fluorine doping of $SrTiO_3$ in 2003.[17] They found that in the photocatalytic NO oxidation, F-doped $SrTiO_3$ showed higher activity than the pure material by three times at wavelengths longer than 400 nm. Ohno *et al*. reported that, compared with pristine $SrTiO_3$, the absorption edge of S and C doped $SrTiO_3$ was greatly shifted from 400 to 700 nm. Moreover, S and C doped $SrTiO_3$ showed photocatalytic activity under visible light in 2-propanol decomposition. [19]

Nitrogen doped $SrTiO_3$ was first reported by Wang *et al.*.[20] They observed that for NO oxidation, the photocatalytic activity of N-doped $SrTiO_3$ is about 3.5 times higher than that of pure $SrTiO_3$. Zou *et al.* found that nitrogen-doped mesoporous $SrTiO_3$ was able to decompose model dye compounds like RhB, methyl orange and MB under pure visible light irradiation (λ> 420 nm).[23]

At the meantime, the effect of non-metal doping on electronic structure of $SrTiO_3$ has been investigated by density-functional theoretical (DFT) calculations.[25-31] Mi *et al.* found that the visible light absorption of N-doped $SrTiO_3$ results from the localized N 2p states above the valence band maximum (VBM) mainly composed of O 2p bands.[25] Jia and co-workers investigated geometric and electronic structures of B, C, N, F, P, S doped $SrTiO_3$ systems and found that only in S-doped case, the S 3p states mix well with the O 2p states and lift the energy level of VBM which narrows the band gap narrower.[29] Liu *et al.* reported that based on the electronic band position and optical absorption study, co-doped (N-N, N-P, N-S and P-P) $SrTiO_3$ were predicted to be promising materials for the visible-light photocatalysis.[30] However, to our knowledge, all of the reported theoretical studies of non-metal doping $SrTiO_3$ are focused on the bulk material.

Since many reactivity properties of photocatalytic materials are influenced to a large extent by surface processes, analysis of the doping characteristics at surfaces is of significant relevance. Experimentally, low energy electron diffraction (LEED), medium energy ion scattering (MEIS) and surface X-ray diffraction (SXRD) were applied to investigate the surface structures of $SrTiO_3$.[32-34] The SXRD study at 300 K

on the structure of $SrTiO_3$(001) surface with 78% TiO and 22 % SrO terminations indicated that the structure of Ti atoms on the TiO terminations is in agreement with the MEIS data,[32,33] but is different from the DFT calculations.[35,36] Padilla and Vanderbilt theoretically studied that the surface relaxation and electronic structure of both SrO- and TiO_2-terminated surfaces of $SrTiO_3$. They found that both SrO- and TiO_2-terminated surfaces have a comparable range of thermodynamic stability, showing that either termination can be formed depending on whether growth occurs in Sr-rich or Ti-rich conditions.[35]

In the present work, in order to obtain a comprehensive understanding of non-metal doped $SrTiO_3$ surface, we performed DFT calculations to investigate the effects of doping with non-metal anions X (X=C, N, F, Si, P, S, Cl, Se, Br and I) on the energetic and electronic structure of SrO- and TiO_2-terminated $SrTiO_3$ (001) surfaces. Various substitutional configurations at the surface and subsurface layers were considered. The main aim of this study is to identify and rationalize the trends along the series, to discuss the stability of the different doping cases based on the calculated formation energies, and to explore how the conduction band minimum (CBM) and the valence band maximum (VBM) of pure $SrTiO_3$ surfaces are influenced by the dopants and whether the doping introduces band gap states.

2. Computational Details

All the spin-polarized DFT calculations were performed with the VASP (Vienna Ab initio Simulation Package) code.[37,38] The exchange correlation potential was described by the Perdew-Burke-Ernzerhof (PBE) functional within the generalized gradient

approximation (GGA).[39] The projector-augmented wave method was applied to describe electron-ion interactions.[40,41] Full optimization of the cell parameters for the bulk $SrTiO_3$ with perovskite structure was carried out by using the 9×9×9 Monkhorst-Pack type *k*-point sampling. The cutoff energy for the plane wave basis set was fixed at 400 eV. The geometries were considered to be converged when the forces on each ion become 0.01 eV/ Å or less. The calculated lattice parameters, $a = b = c$ =3.914 Å, are in good agreement with experimental data,[42] and applied in the subsequent calculations of surfaces. For the simulation of surfaces, we employed slab models consisting of five alternating atomic layers with mirror-symmetry to construct the SrO- and TiO_2-terminated $SrTiO_3$ (001) surfaces. The models with a (2×2) periodicity of supercell adopted in our calculations are shown in Fig. 1. A vacuum layer of 12 Å was used in order to avoid the interaction between periodic slabs. The *k*-point sampling was set to be 3×3×1 in the calculation of geometry optimization and 5×5×1 in the computation of electronic properties. The upper three atomic layers were allowed to relax, while the bottom two atomic layers were fixed at its optimized bulk position. Dipolar corrections were included along the axis normal to the surface.

On top of the relaxed geometries obtained at the GGA-PBE level, a more accurate approach, the hybrid functional HSE06 presented by Heyd, Scuseria and Ernzerhof,[43-45] was used to calculate the electronic structure. The HSE06 functional includes a fraction α, of screened, short-range HF exchange to improve the derivative discontinuity of the Kohn-Sham potential for integer electron numbers. The percentage of HF exchange in a hybrid functional is not a universal constant and the

optimal value can be system-dependent. In the present work, an α=0.3 was used as this value can yield an excellent agreement between the computed band gap (3.4 eV) and the experimental result.[46]

3. Results and Discussion

3.1. Bulk $SrTiO_3$ and bare (001) surfaces

$SrTiO_3$ crystallizes in a typical perovskite structure, in which the Sr cation is 12-fold coordinated and the Ti cation is 6-fold coordinated with the oxygen anions, and the corner-sharing TiO_6 octahedra forms the skeleton of the structure, in which the center position is occupied by the Sr cation. So the crystal structure of $SrTiO_3$ with the space group *Pm3m* has been considered in the present study (Fig. 1(a)). The bond length of Ti-O is calculated to be 1.957 Å. The shortest distance of Sr and O is computed to be 2.767 Å and the shortest distance of Ti and Si is predicted to be 3.389 Å. As shown in Fig. 1(b), for the relaxed SrO-terminated $SrTiO_3$ (001) surface, the shortest distances between Sr atom in the first layer and O atoms in the first and second layer are 2.776 and 2.637 Å, respectively. The bond lengths between Ti atom in the second layer and O atoms in the first and second layer are 1.945 and 1.957 Å, respectively. The shortest distance between Sr atom in the first layer and Ti atom in the second layer is computed to be 3.262 Å. As can be found from Fig. 1(c), for the optimized TiO_2-terminated $SrTiO_3$ (001) surface, the bond lengths between Ti atom in the first layer and O atoms in the first and second layer are 1.959 and 1.874 Å, respectively. The shortest distances between Sr atom in the second layer and O atoms in the first and second layer are 2.683 and 2.771 Å, respectively. The calculated

shortest distance between Ti atom in the first layer and Sr atom in the second layer is computed to be 3.270 Å. Our calculation shows that compared with the geometrical parameters in bulk structure, the structure in horizontal plane of (001) surface seldom changes while the vertical distance between the first two layers shrinks.

Fig. 2 displays the calculated total density of states (TDOS) and partial density of states (PDOS) for $SrTiO_3$ bulk and (001) surfaces by HSE06 method. We can see that the band gap of bulk $SrTiO_3$ is computed to be 3.4 eV, which is equal to the experimental result.[46] Fig. 2(a) indicates that the VBM of bulk $SrTiO_3$ is principally O 2p states in character and CBM is mainly composed of Ti 3d states. Generally, one expects a decrease in the band gap of the surface compared with the bulk value due to the dangling bonds existing on the surface. As shown in Fig. 2(b), the band gap of SrO-terminated (001) surface is 3.34 eV, which is slightly smaller than that of bulk. PDOSs suggest that the slight decrease of the band gap mostly results from the sublayer Ti 3d states. The calculated band gap of TiO_2-terminated (001) surface is 2.56 eV, which is remarkably narrower than the bulk value. As can be seen from PDOSs in Fig. 2(c), new surface states in the VBM are primarily composed of surface O 2p states.

3.2. Formation energy

We have considered two different configurations for each doped system by substituting a non-metal atom for the O atom in the first and second layer shown in Fig. 1, respectively. To probe the relative stability of X-doped $SrTiO_3$ structures, the defect formation energies (E_f) of substitutionally doped systems are estimated

according to the following equation

$$E_f = E_{X-doped} + \mu_O - E_{undoped} - \mu_X \qquad (1)$$

where $E_{X-doped}$ and $E_{undoped}$ are total energies of the supercells with and without dopants, respectively. The quantities μ_O and μ_X represent the chemical potential for oxygen and X atoms, respectively. The chemical potential of O depends on the nature of synthesis conditions of $SrTiO_3$. Under the conditions of equilibrium between the $SrTiO_3$ and the reservoirs of Sr, Ti and O, their chemical potentials must follow the relation

$$\mu_{Sr} + \mu_{Ti} + 3\mu_O = \mu_{SrTiO3(bulk)} \qquad (2)$$

The chemical potentials of the elements Sr, Ti and O cannot exceed the corresponding chemical potential in the bulk. Thus, one has $\mu_{Sr} \leq \mu_{Sr(bulk)}$, $\mu_{Ti} \leq \mu_{Ti(bulk)}$, $\mu_O \leq \mu_{O(gas)}$. Under the O-rich limit, μ_O is calculated from the energy of an oxygen atom in the gaseous O_2 molecule placed at the center of a 15 × 15 × 15 $Å^3$ cubic box. Under the metal-rich limit, μ_{Sr} and μ_{Ti} are calculated from the energy of the respective atoms in their pure bulk metallic states, and μ_O is determined using eqn (2).[31,47] The chemical potential μ_X is obtained from the energy calculated for one X atom in a cubic unit cell with side length of 15Å. The calculated formation energies in X-doped systems are summarized in Table 1.

It is noted from Eq (1) that the substitutional doping is energetically more favorable as the E_f value becomes smaller. From the E_f value of Table 1, the following trends are observed:

(a) The doping is energetically favored under metal-rich growth condition with

respect to the O-rich growth condition.

(b) The doping is energetically more favorable in the first layer than the second layer for both terminations except N-doped SrO-terminated $SrTiO_3$ (001) surface.

(c) For the doping in the first layer, X (X=C, N and F) atom with relatively smaller atom radius tends to substitute the O atom in the TiO_2-terminated surface while the preferential occupation of the X(X=P, S, Cl, Se and Br) atom with larger atom radius takes place at the O position in the SrO-terminated surface.

(d) As to the substitution of non-metal atom in the second layer, the doping configuration for TiO_2-terminated surface is easier to form than that for SrO-terminated surface except the F-doped system.

The X-doped system with smaller formation energy indicated that it is the more probable occurring defective configurations in experiments. Given this, we shall only discuss the details of structural and electronic properties for the doping cases in the first layer of SrO- and TiO_2-terminated $SrTiO_3$ (001) surfaces.

In order to prove the rationality of our current model, we chose a larger supercell including seven atomic layers to calculate the formation energy for each impurity case.[48] The results are shown in parentheses in Table 1. As can be seen, for the doping in the first layer, the defect formation energy is seldom affected by the thickness of supercells (within 0.1 eV), especially for the element with relatively smaller atomic radius, such as C and N. For the doping in the second layer, the obvious change of the defect formation energy is observed as the thickness of atomic layers increases,

especially for the SrO-terminated surface doped with Br and I. Nevertheless, compared with the supercell with five atomic layers, a supercell including seven atomic layers produces the same trend on the most stable doping site for every system. Therefore, we will use the current model including five atomic layers to discuss the geometrical and electronic structures.

3.3. Doping in the SrO-terminated $SrTiO_3$ (001) surface

The optimized partial geometrical structures are shown in Fig. 3. The calculated TDOS and PDOS for doped systems are displayed in Figure 4 and 5, where the zero energy value is set at the top of the valence band for pure surface in order to easily allow identification of the band gap and of the relative position of the impurity states introduced by dopants.

As shown in Fig. 3, replacing one surface O atom with non-metal atom X induces the different degrees of distortion in the local structure around the Ti atom bonding to dopants. For all the doped systems, the distance between X atom and Ti atom is calculated to be longer than that between the surface O atom and Ti atom (1.945 Å) in the pure surface. The Ti atom bonded to X atom moves downward to decrease the bond length of Ti atom and the O atom in the third layer compared with the value in the pure surface (2.039 Å) except N-doped system. The larger the radius of doping atom in the same main group, the longer the distance: 3.161 Å for Ti-Si > 2.242 Å for Ti-C, 3.161 Å for Ti-P > 3.185 Å for Ti-N, 3.161 Å for Ti-Se > 2.868 Å for Ti-S, and 3.898 Å for Ti-I > 3.545 Å for Ti-Br 3.290 Å for Ti-Cl > 2.438 Å for Ti-F. The Ti atom bonded to X atom pulls the adjacent O atoms in the second layer, which results

in the bond length of Ti-O shorter than that in the bare surface (1.957 Å) for most of doped cases, such as, 1.948 Å for X=C, 1.936 Å for X=Si, 1.940 Å for X=F and 1.935 Å for X=I. Among all the X-doped systems, the introduction of N atom is founded to cause the least change of local structure due to its similar radius to the O atom. Combined with the lowest defective formation energy, the N-doped SrO-terminated $SrTiO_3$ (001) surface is most likely to be formed, which is indeed the subject of extensive experimental studies.[20-23]

Generally, replacing O atoms with other non-metal elements will influence the electronic structures of semiconductors.[49-52] As shown in Fig. 4(a) and 4(b), the C-doping introduces three band gap states of C 2p orbital character in the spin-up and spin-down bands. The calculated Fermi-level is at 1.59 eV above the VBM. Therefore, the two up-spin gap states are occupied, while the down-spin gap state is unoccupied, so that there is a magnetic moment of 2.0 μ_B per carbon as reported earlier for C-doped TiO_2.[53,54] There is no change of the band gap for C doping with respect to the pure $SrTiO_3$ surface. Similarly, for Si-doped system, substitution of Si at the surface O site results in little shift of the position of the VBM and CBM. The Fermi energy is set at 3.12 eV above the VBM and two occupied Si 3d states in the middle of the band gap are below the Fermi level while the other one is located above the Fermi level, which leads to a magnetic moment of 2.0 μ_B per silicon.

As can be seen from Fig. 4(a) and 4(b), the N 2p orbitals split into occupied and unoccupied states, mixing well with O 2p orbitals near the VBM and located at the "forbidden gap" near to the CBM. We believe that a higher concentration of N results

in the formation of continuum states at the band edges, like the obtained results in bulk structure.[31] As the unoccupied states are close to the CBM, we assume that the band gap is the difference between the lowest unoccupied states and the highest occupied states, and calculated to be 2.29 eV. For subsitutional P to O doping, Fig. 4 shows little shift of the position of the VBM and CBM with respect to the undoped material. The Fermi level is computed to be at 1.53 eV. The most of P 3p states lie in the band gap and form three occupied and one unoccupied energy bands.

Since the total number of electrons remain the same after replacing O with S or Se atom, the overall VBM and CBM profiles look spin-symmetric and clean for both S-doping and Se-doping cases as indicated in Fig. 4. For both cases, the impurity states of dopants are close to the VBM. The VBM edge of S-doped system is shifted upwards by 0.19 eV and mainly composed of the S 3p orbitals, whereas the CBM remains almost unchanged. Thus, the effective band gap of S-doped system is 3.15 eV. For Se-doped surface, the highest occupied energy level moves upwards significantly by 0.57 eV, due to the much higher energy of Se 4p compared to the O 2p orbitals. While the CBM keeps almost at its original position. Consequently, the calculated band gap of Se-doped case is 2.77 eV.

The effect of an X-dopant (X=F, Cl, Br and I) on the electronic structure can be found from Fig. 5. Several experimental investigations showed that there is no change in the optical adsorption edge of oxides upon F-doping since the F 2p orbitals are lower in energy than the O 2p orbitals.[55-57] Our results suggest that for SrO-terminated $SrTiO_3$ (001) surface, doping F also does not change the initial positions of the VBM

and CBM. For Cl-doped system, the band gap also remains the value in pure surface. For subtitutional Br to O, the highest occupied Br 4p states locate just above the VBM and well overlap with O 2p states. As a result, new edge of valence band shifts towards the higher energy by 0.56 eV. The position of CBM is seldom affected. Then, the effective band gap of Br-doped case is 2.78 eV. As shown in Fig. 5(a) and 5(b), the VBM of I-doped system is raised from that of pure surface by 0.58 eV due to the contribution of I 5p states, and the CBM keeps at the original position, which results in the band gap of 2.76 eV.

3.4. Doping in the TiO_2-terminated $SrTiO_3$ (001) surface

Fig. 6 shows the relaxed partial geometries for TiO_2-terminated surface models doped with non-metal elements. The side view of local structure looks like a square. As indicated in Fig. 6, the doping atoms with bigger atomic radius result in the larger distortion. The dopant X (X=Si, P, S, Se, C, Br and I) moves upwards more remarkably than X (X=C, N and F). The bond length of Ti-X for every X-doped system is longer than that of Ti-O (1.959 Å) in the pure surface. In the same vertical column in the periodic table of elements, the larger atomic number the doping element, the longer the bond length of Ti-X: Ti-Si (2.546 Å) > Ti-C (2.546 Å), Ti-P (2.444 Å) > Ti-N (1.996 Å), Ti-Se (2.499 Å) > Ti-S (2.362 Å), Ti-I (2.886 Å) > Ti-Br (2.660 Å) > Ti-Cl (2.505 Å) > Ti-F (2.071 Å). This phenomenon suggests that the incorporation of the larger atom in the surface O site yields more strains to the neighboring Ti atoms compared with the smaller atom, which is also found in the bulk structure.[29] The other obvious deformation is that the O atoms in the second layer moves inwards and the

degree of movement is directly related to the size of the doping atom. Interestingly, for the X-doped systems (X=C, Si, N, P, S and Se), the bond length of Ti and O atom in the second layer becomes longer than that of Ti-O (1.874 Å) in the bare surface due to the moving outwards of Ti atoms bonded to the X atom. While for the X-doped cases (X=F, Cl, Br and I), the bond length of Ti and O atom in the second layer is shorter than that of Ti-O bond in the clean surface due to the moving downwards of Ti atoms bonded to the X atom. In the pure TiO_2-terminated $SrTiO_3$ (001) surface, the bond length of O atom in the second layer and Ti atom in the third layer is calculated to 2.005 Å, which undergoes varying degrees of change (-0.031 Å ~ +0.112 Å) depending on the atomic radius of dopant. Like the case in SrO-terminated surface, N-doped system brings the smallest distortion to the local structure owing to the atomic radius of N similar to that of O.

To investigate the origin of the X-doping (X=C, N, F, Si, P, S, Cl, Se, Br, and I) effect on the electronic property of TiO_2-termiation, the TDOS and PDOS of X-doped surfaces are calculated and plotted in Fig. 7 and 8. As shown in Fig. 7(a) and (b), the C-doping has no significant effects on the position of the VBM and CBM, and introduces two gap states. The highest energy level of spin-up and spin-down states are 0.45 and 1.26 eV above the VBM, respectively. They are occupied since the Fermi level is at 1.3 eV above the VBM. C 2p states not only essentially contribute to these gap states but also spin-polarization of energy levels in the VBM and CBM. For the Si-doped system, our finding is that the VBM keeps the position of pure surface, and some gap states are located close to the CBM, which mostly comprise the Si 3p states

as shown in Figure 7(b). The lowest energy level of these gap states is 0.88 eV below the CBM. In addition, the Fermi level is pinned in the conduction band edge above the CBM about 0.12 eV, indicating n-type characteristic of semiconductor. The similar property was also found in Si-doped TiO_2.[58]

Fig. 7 shows that replacing the surface O atom with N atom does not cause any obvious change in the positions of VBM and CBM of TiO_2-terminated surface. Most of the N 2p states well mix with O 2p states in the valence band and some unoccupied states are located in the conduction band. In the case of P-doped surface, the VBM displays little movement while the CBM moves to a lower energy level by about 0.3 eV compared with the pure surface. The PDOS shows that most of the P 3p states are located in and near the VBM and some of them lie below the CBM.

For the S-doped case, our results show little shift of the position for the VBM while there is a slight downward movement (0.1 eV) of the CBM compared to the undoped surface. Some of the S 3p states overlap with the valence band of surface and others extend into the band gap with a maximum about 0.71 eV above the VBM. The calculated Fermi level is right above these S 3p states. The excitations from these occupied S 3p states to the conduction band may induce obvious red-shift of absorption edge. For the Se-doped model, the TDOS in Fig. 7(a) shows that the impurity states lie above the VBM and in the middle of gap, while the PDOS indicates that the impurity states are mainly composed of Se 4p orbitals. Some of Se 4p states extend in energy into the band gap with a maximum of about 1.3 eV from the VBM, leading the Fermi level, to locate above the localized states. Thus, the transition from

these occupied Se 4p states to the conduction band may lead to a decrease in the photon excitation energy and result in an obvious red-shift of the absorption edge.

As shown in Fig. 8(a), the profile of TDOS for every halogen doping case looks similar. The calculated band gap is 1.94 eV for F-doped one, 1.92 eV for Cl-doped one, 1.91 eV for Br-doped one and 1.91 eV for I-doped one. Compared with the bare surface, the position of VBM maintains while there is an obvious decline of the CBM. Fig. 8(b) indicates that most of X (X=F, Cl, Br and I) np states are located below the surface O 2p states, which results in little effect on the position of VBM. Since halogen is monovalent, after doping, the extra electron formally belonging to the O atom which has been replaced must be transferred to the empty Ti states. Such electron is found to be self-trapped at one Ti site in a $3d_{xy}$ state which is separated by the bottom of the conduction band by about 0.8 eV for TiO_2.[52] This is the typical position of the impurity states which appear in the band gap of TiO_2 upon chemical reduction and formation of Ti^{3+} states. In our results, the lowest energy level of these Ti 3d states is located below CBM by around 0.6 eV, which leads to the band gap narrowing.

3.5. Prediction on photocatalytic applications

In the photocatalytic overall water-splitting reactions, the photo-genenerated electrons and holes cause redox reactions similarly to electrolysis. Water molecules are reduced by the electrons to form H_2 and are oxidized by the holes to from O_2. Important points in the semiconductor photocatalyst materials are the width of the band gap and levels of the conduction and valence bands. To make efficient use of the

visible light, the semiconductor band gap should be smaller than 3.0 eV. The CBM has to be more negative than the reduction potential of H^+/H_2 (0 V vs. NHE), whereas the VBM has to be more positive than the oxidation potential of O_2/H_2O (1.23 V). In order to evaluate the physical significance of this work, the calculated results and analysis are presented in the form of schematic diagram in Figure 9. According to experimental measurements,[46] the rough conduction band edge potential of $SrTiO_3$ is -1.26 V with respect to NHE. Subsequently the valance band edge position is determined as 2.14 V based on the calculated band gap of 3.4 eV. To assess the photocatalytic performance, we have aligned the CBM and VBM energy levels of X-doped SrO- and TiO_2-terminated $SrTiO_3$ (001) surfaces obtained from the corresponding TDOS plots by taking into account the relative location with respect to the undoped $SrTiO_3$.

As shown in Figure 9(a), for SrO-terminated surface, some impurity states are localized in the middle of band gap in C-, Si- and P-doped systems, which are detrimental for photocatalysis because the gap states can act as recombination centers to limit the efficiency of semiconductors. For N-doped case, due to the appearance of impurity states near to the CBM and VBM, the band gap is reduced to 2.29 eV and the photo-reduction and photo-oxidation capabilities are predicted to be improved, which is in good agreement with the experimental observation.[23] Doping with isovalent elements (S and Se) essentially influences the position of VBM and enhances the photo-oxidation capacity. For Se-doped system, the absorption edge moves from UV to visible light range. As to halogen doping, replacing O with F and Cl exerts no effect

on the band-gap narrowing. For Br- and I-doped systems, photo-oxidation abilities are improved since the position of CBM moves towards the energy levels of water oxidation while the position of VBM maintains.

Figure 9(b) indicates that the band gap of pure TiO_2-terminated surface is 2.56 eV, which corresponds to the visible light absorption, and the position of VBM moves upwards compared with the bulk. In other words, exposing TiO_2-terminated (001) surface is not only in favor of absorbing visible light and but also helpful for improving the photo-oxidation ability. C, Si and P dopings create localized states detached from the CBM and VBM, which can act as recombination centers, having adverse effect on the photocatalytic activity. Substituting O atom with N atom has no influence on the narrowing of band gap because the N 2p states overlap with the surface atomic states. Replacing O with S or Se induces new states in the band gap associated with the S 3p or Se 4p level. This should strongly reduce the energy required to excite electrons from these states into the CBM, but might accelerate the charge carrier recombination rate due to the rather localized nature of the new states. Doping halogen essentially decreases the CBM level, improves the ability of photo-reduction, and extends the visible light absorption.

Combining the calculated results of SrO-termination with those of TiO_2-termination, we propose that N-doped, Br-doped and I-doped $SrTiO_3$ (001) surfaces can not only extend the absorption edge to the visible light region but also improve the ability of photo-oxidation and/or photo-reduction. Several experimental studies have already focused on the N-doped $SrTiO_3$, which indeed shows the photocatalytic activity under

visible light irradiation. Further experiments should therefore be done for Br-doped and I-doped $SrTiO_3$ to systemically investigate their photocatalytic properties.

4. Conclusions

We have investigated here the effect of anion-doping on the surface structure, electronic structure and photocatalytic performance of $SrTiO_3$ (001) surface with different terminations by using DFT calculations. Some conclusions are remarked:

(1) The anion-doping is energetically more favorable in the top layer than the sublayer for most of X-doped systems, and favored under metal-rich limit with respective to the O-rich limit.

(2) X (X=C, N and F) atom with relatively smaller atom radius tends to substitute the O atom in the TiO_2-terminated surface while the preferential occupation of the X(X=P, S, Cl, Se and Br) atom with larger atom radius takes place at the O position in the SrO-terminated surface.

(3) Exposing pure TiO_2-terminated surface is not only in favor of absorbing visible light and but also helpful for improving the photo-oxidation ability.

(4) Replacing O with C, Si, and P creates localized states detached from the CBM and VBM, which can act as recombination centers, detrimental for photocatalysis.

(5) Replacing O with S or Se induces new states in the band gap, which can reduce the energy required to excite electrons from these states into the CBM, but might accelerate the charge carrier recombination rate.

(6) N-doped, Br-doped and I-doped $SrTiO_3$ (001) surfaces are promising for photocatalytic applications in the visible light region owing to the remarkably narrowed band gap and increased photocatalytic reduction or oxidation ability compared with the pure surface.

Acknowledgements

Dr. Dong gratefully acknowledges the financial support from the National Science Foundation of China under Grant 21303079. Dr. Zhou appreciates the funding support by the National Natural Science Foundation of China under Grant 21473183.

References

1 K. Maeda and K. Domen, *J. Phys. Chem. C*, 2007, **111**, 7851-7861.

2 P. V. Kamat, *J. Phys. Chem. C*, 2007, **111**, 2834-2860.

3 A. Kudo and Y. Miseki, *Chem. Soc. Rev.*, 2009, **38**, 253-278.

4 Y. Inoue, *Energy Environ. Sci.*, 2009, **2**, 364-386.

5 K. Maeda and K. Domen, *J. Phys. Chem. Lett.*, 2010, **1**, 2655-2661.

6 X. Chen, S. Shen, L. Guo and S. S. Mao, *Chem. Rev.*, 2010, **110**, 6503-6570.

7 K. Domen, A. Kudo and T. Onishi, *J. Catal.*, 1986, **102**, 92-98.

8 M. Shibata, A. Kudo, A. Tanaka, K. Domen, K. Maruya and T. Ohishi, *Chem. Lett.*, 1987, **16**, 1017-1018.

9 R. Abe, M. Higashi, Z. Zou, K. Sayama and Y. Abe, *Chem. Lett.*, 2004, **33**, 954-964.

10 R. Abe, M. Higashi, K. Sayama, Y. Abe and H. Sugihara, *J. Phys. Chem. B*, 2006, **110**, 2219-2226.

11 Y. Miseki, H. Kato and A. Kudo, *Energy Environ. Sci.*, 2009, **2**, 306-314.

12 K. Iwashina and A. Kudo, *J. Am. Chem. Soc.*, 2011, **133**, 13272-13275.

13 S. X. Ouyang, H. Tong, N. Umezawa, J. Cao, P. Li, Y. P. Bi, Y. J. Zhang and J. H. Ye, *J. Am. Chem. Soc.*, 2012, **134**, 1974-1977.

14 X. Wang, K. Maeda, A. Thomas, K. Takanabe, G. Xin, J. M. Carlsson, K. Domen

and M. Antonietti, *Nat. Mater.*, 2009, **8**, 76-80.

15 K. Kalyanasundaram, E. Borgarello, D. Duonghong and M. Graetzel, *Angew. Chem., Int. Ed. Engl.*, 1981, **20**, 987-988.

16 X. B. Chen, L. Liu, Y. Y. Peter and S. S. Mao, *Science*, 2011, **331**, 746-750.

17 J. Wang, S. Yin, Q. Zhang, F. Saito and T. Sato, *Chem. Lett.,* 2003, **32**, 540-541.

18 J. Wang, S. Yin, Q. Zhang, F. Saito and T. Sato, *Solid State Ionics*, 2004, **172**, 191-195.

19 T. Ohno, T. Tsubota, Y. Nakamura and K. Sayama, *Appl. Catal. A*, 2005, **288**, 74-79.

20 J. Wang, S. Yin, M. Komatsu, Q. Zhang, F. Saito and T. Sato, *J. Photochem. Photobiol. A*, 2004, **165**, 149-156.

21 J. Wang, S. Yin, M. Komatsu, Q. Zhang, F. Saito and T. Sato, *Appl. Catal. B*, 2004, **52**, 11-21.

22 U. Sulaeman, S. Yin and T. Sato, *J. Nanomater.*, 2010, **2010**, 629727/1–6.

23 F. Zou, Z. Jiang, X. Qin, Y. Zhao, L. Jiang, J. Zhi, T. Xiao and P.P. Edwards, *Chem. Commun.* 2012, **48**, 8514-8516.

24 J. Wang, H. Li, H. Li, S. Yin and T. Sato, *Solid State Sci.* 2009, **11**, 182-188.

25 Y. Y. Mi, S. J. Wang and Y. P. Feng, *Appl. Phys. Lett.*, 2006, **89**, 231922.

26 N. Li and K. L. Yao, *AIP Advances*, 2012, **2**, 032125/1-10.

27 H. F. Liu, *Solid State Communications*, 2012, **152**, 2063-2065.

28 C. Zhang, Y. Jia, Y. Jing, Y. Yao, J. Ma and J. Sun, *Physica B*, 2012, **407**, 4649-4654.

29 C. Zhang, Y. Jia, Y. Jing, Y. Yao, J. Ma and J. Sun, *Comput. Mater. Sci.*, 2013, **79**, 69-74.

30 P. Liu, J. Nisar, B. Pathak and R. Ahuja, *Inter. J. Hydrogen Energy*, 2012, **37**, 11611-11617.

31 B. Modak, K. Srinivasu and S. K. Ghosh, *Phys. Chem. Chem. Phys.*, 2014, **16**, 24527- 24535.

32 N. Bickel, G. Schmidt, K. Heinz and K. Müller, *Phys. Rev. Lett.*, 1989, **62**, 2009-2011.

33 A. Ikeda, T. Nishimura, T. Moishita and Y. Kido, *Surf. Sci.*, 1999, **433**, 520-524.

34 G. Charlton, S. Brennam, C. A. Muryn, R. McGrath, D. Norman, T. S. Turner and G. Thornton, *Surf. Sci.*, 2000, **457**, L376-L380.

35 J. Padilla and D. Vanderbilt, *Surf. Sci.*, 1998, **418**, 64-70.

36 Z.-Q. Li, J.-L. Zhu, C. Q. Wu, Z. Tang and Y. Kawazoe, *Phys. Rev. B*, 1998, **58**, 8075- 8078.

37 G. Kresse and J.Furthmüller, *Phys. Rev. B*, 1996, **54**, 11169-11186.

38 G. Kresse and J.Furthmüller, *Comput. Mater. Sci.*, 1996, **6**, 15-50.

39 J. P. Perdew, K. Burke and M.Ernzerhof, *Phys. Rev. Lett.*, 1996, **77**, 3865-3868.

40 P. E. Blochl, *Phys. Rev. B*, 1994, **50**, 17953-17979.

41 G. Kresse and J. Joubert, *Phys. Rev. B*, 1999, **59**, 1758-1775.

42 Y. A. Abramov, V. G. Tsirelson, V. E. Zavodnik, S. A. Ivanov and I. D. Brown, *Acta Crystallogr. B*, 1995, **51**, 942-951.

43 J. Heyd, G. E. Scuseria and M. Ernzerhof, *J. Chem. Phys.*, 2003, **118**, 8207-8215.

44 J. Heyd, G. E. Scuseria and M. Ernzerhof, *J. Chem. Phys.*, 2004, **121**,1187-1192.

45 J. Heyd, G. E. Scuseria and M. Ernzerhof, *J. Chem. Phys.*, 2006, **124**, 219906.

46 Y. Xu and M. A. A. Schoonen, *Am. Mineral.*, 2000, **85**, 543-556.

47 J. A. Dawson, H. Chen and I. Tanaka, *J. Phys. Chem. C*, 2014, **118**, 14485-14494.

48 K. Johnston, M. R. Castell, A. T. Paxton and M. W. Finnis, *Phys. Rev. B*, 2004, **70**, 085415.

49 K. Yang, Y. Dai, B. Huang and M.-H. Whangbo, *Chem. Mater.*, 2008, **20**, 6528-6534.

50 R. Long, N. J. English and Y. Dai, *J. Phys. Chem. C*, 2009, **113**, 17464-17470.

51 M. Nolan, R. Long, N. J. English, D. A. Mooney, *J. Chem. Phys.*, 2011, **134**, 224703-1-8.

52 C. Di Valentin and G. Pacchioni, *Catal. Today*, 2013, **206**, 12-18.

53 H. Kamisaka, T. Adachi and K. Yamashita, *J. Chem. Phys.*, 2005, **123**, 084704-1-084704-9.

54 K. Yang, Y. Dai, B. Huang and M.-H. Whangbo, *J. Phys. Chem. C*, 2009, **113**, 2624- 2629.

55 N. Todorova, T. Giannakopoulou, G. Romanos, T. Vaimakis, J. Yu and C. Trapalis, *Int. J. Photoenergy*, 2008, 534038.

56 A. M. Czoska, S. Livraghi, M. Chiesa, E. Giamello, S. Agnoli, G. Granozzi, E. Finazzi, C. Di Valentin and G. Pacchioni, *J. Phys. Chem. C*, 2008, **112**, 8951-8956.

57 X. Nie, S. Zhuo, G. Maeng, K. Sohlberg and Trapalis, *Int. J. Photoenergy*, 2009, 294042.

58 K Yang, Y. Dai and B. Huang, *Chem. Phys. Lett.*, 2008, **456**, 71-75.

59 Y. Xu and M. A. A. Schoonen, *American Mineralogist*, 2000, **85**, 543-556.

Table 1 Calculated defect formation energies in SrO- and TiO_2-terminated $SrTiO_3$ (001) surfaces under O-rich and metal-rich conditions. The data in parentheses are obtained from supercells including seven atomic layers.

E_f (eV)	SrO-first O-rich	SrO-first metal-rich	SrO-second O-rich	SrO-second metal-rich	TiO_2-first O-rich	TiO_2-first metal-rich	TiO_2-second O-rich	TiO_2-second metal-rich
C	-1.07 (-1.07)	-6.25 (-6.25)	-0.47(-0.50)	-5.66 (-5.69)	-1.51 (-1.49)	-6.70 (-6.68)	-1.18 (-1.16)	-6.37 (-6.40)
N	-2.90 (-2.90)	-8.09 (-8.09)	-3.14 (-3.14)	-8.33 (-8.33)	-3.60 (-3.59)	-8.79 (-8.78)	-3.56 (-3.52)	-8.75 (-8.71)
F	-2.82 (-2.86)	-8.01 (-8.05)	-2.05 (-2.04)	-7.24 (-7.23)	-2.95 (-3.02)	-8.14 (-8.21)	-2.00 (-2.07)	-7.19 (-7.26)
Si	0.96 (0.94)	-4.23 (-4.25)	5.52 (5.30)	0.33 (0.11)	0.57 (0.52)	-4.62 (-4.67)	4.18 (4.16)	-1.01 (-1.02)
P	-0.89 (-0.93)	-6.07 (-6.12)	3.18 (3.04)	-2.01 (-2.15)	-0.73 (-0.72)	-5.92 (-5.91)	2.13 (2.11)	-3.06 (-3.08)
S	-2.89 (-2.91)	-8.08 (-8.10)	1.09 (0.95)	-4.10 (-4.24)	-1.61 (-1.61)	-6.80 (-6.80)	0.23 (0.18)	-4.96 (-5.01)
Cl	-1.41 (-1.47)	-6.60 (-6.66)	2.92 (2.67)	-2.27 (-2.52)	-0.75 (-0.84)	-5.94 (-6.03)	2.05 (1.94)	-3.14 (-3.25)
Se	-2.14 (-2.16)	-7.33 (-7.35)	3.18 (2.95)	-2.01 (-2.24)	-0.78 (-0.78)	-5.97 (-5.97)	2.07 (2.02)	-3.12 (-3.17)
Br	-0.82 (-0.88)	-6.01 (-6.07)	5.27 (4.65)	0.08 (-0.53)	-0.10 (-0.18)	-5.29 (-5.37)	3.81 (3.68)	-1.38 (-1.51)
I	-0.13 (-0.22)	-5.32 (-5.41)	8.03 (7.55)	2.84 (2.36)	0.59 (0.50)	-4.60 (-4.69)	6.31 (6.18)	1.12 (0.99)

Figure captions

Fig. 1 Bulk structure $SrTiO_3$ (a), slab models of the SrO- (b) and TiO_2-terminated (c) $SrTiO_3$ (001) surface. The green, in gray and red spheres represent Sr, Ti and O atoms, respectively.

Fig. 2 Density of states for the (a) bulk $SrTiO_3$, (b) SrO-terminated $SrTiO_3$ (001) surface and (c) TiO2-terminated $SrTiO_3$ (001) surface. The Fermi level is shown by the vertical dashed line.

Fig. 3 Partial structures of optimized configuration for (a) C-doped, (b) Si-doped, (c) N-doped, (d) P-doped, (e) S-doped, (f) Se-doped, (g) F-doped, (h) Cl-doped, (i) Br-doped, and (j) I-doped SrO-terminated $SrTiO_3$ (001) surface.

Fig. 4 Total density of states (a) and projected density of states (b) for C-doped, Si-doped, N-doped, P-doped, S-doped and Se-doped systems. The vertical dashed line represents the top of the valence band of pure SrO-terminated $SrTiO_3$ (001) surface as the reference level.

Fig. 5 Total density of states (a) and projected density of states (b) for F-doped, Cl-doped, Br-doped, and I-doped systems. The vertical dashed line represents the top of the valence band of pure SrO-terminated $SrTiO_3$ (001) surface as the reference level.

Fig. 6 Partial structures of optimized configuration for (a) C-doped, (b) Si-doped, (c) N-doped, (d) P-doped, (e) S-doped, (f) Se-doped, (g) F-doped, (h) Cl-doped, (i) Br-doped, and (j) I-doped TiO_2-terminated $SrTiO_3$ (001) surface.

Fig. 7 Total density of states (a) and projected density of states (b) for C-doped, Si-doped, N-doped, P-doped, S-doped and Se-doped systems. The vertical dashed line represents the top of the valence band of pure TiO_2-terminated $SrTiO_3$ (001) surface as the reference level.

Fig. 8 Total density of states (a) and projected density of states (b) for F-doped, Cl-doped, Br-doped, and I-doped systems. The vertical dashed line represents the top of the valence band of pure TiO_2-terminated $SrTiO_3$ (001) surface as the reference level.

Fig. 9 Schematic representation of the calculated VBM and CBM position of X-doped SrO- (a) and TiO_2-terminated (b) (001) $SrTiO_3$ surfaces with reference to those of pure $SrTiO_3$.

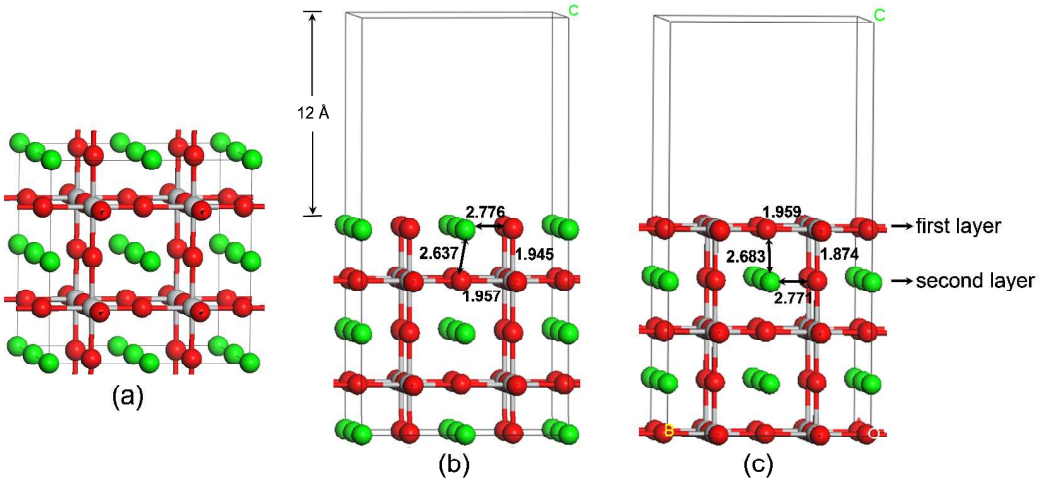

Fig. 1

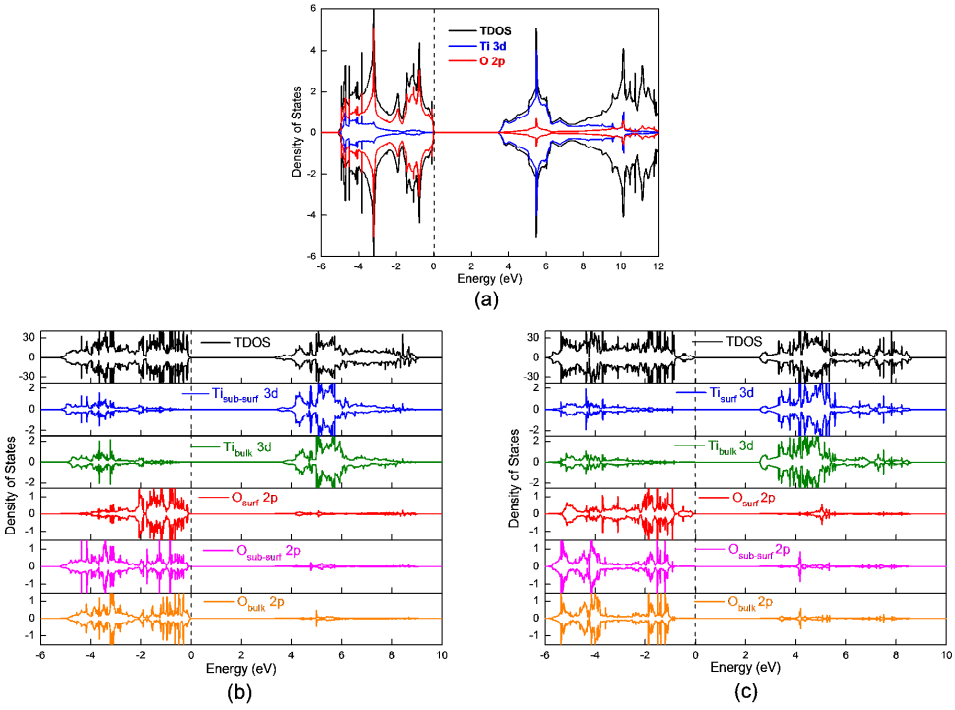

Fig. 2

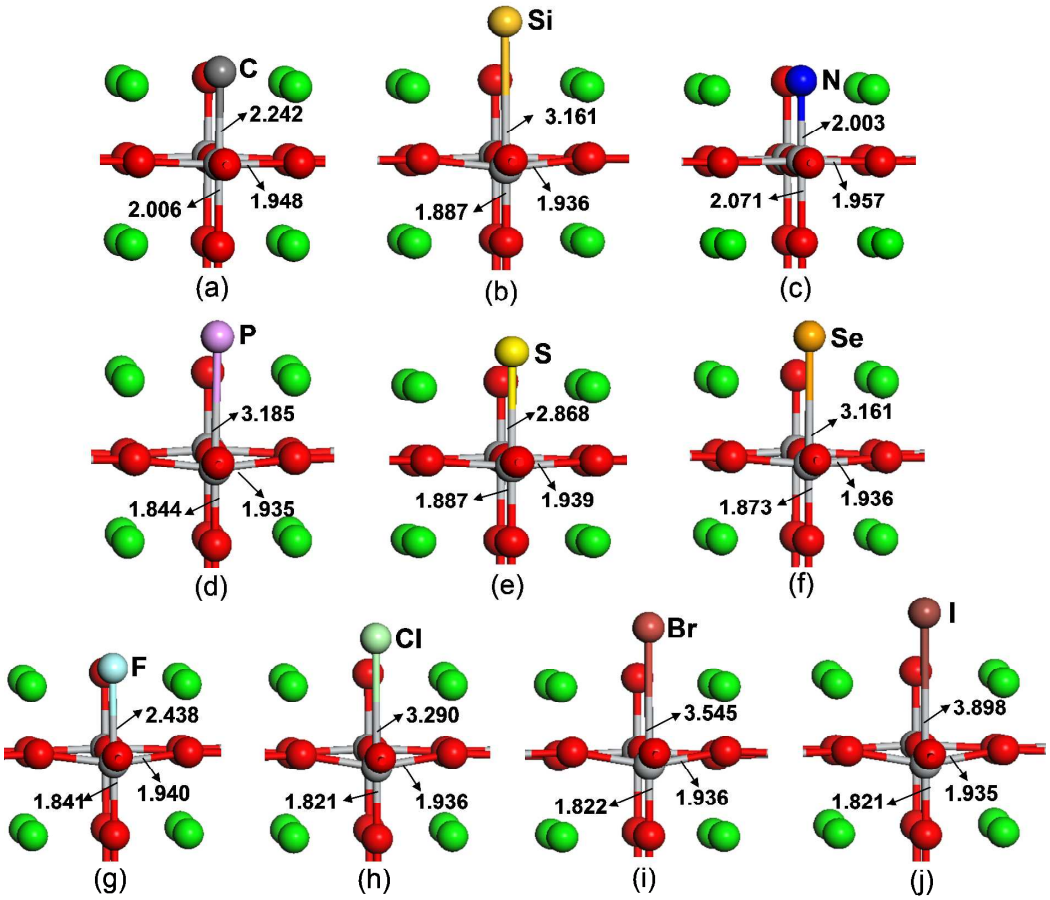

Fig. 3

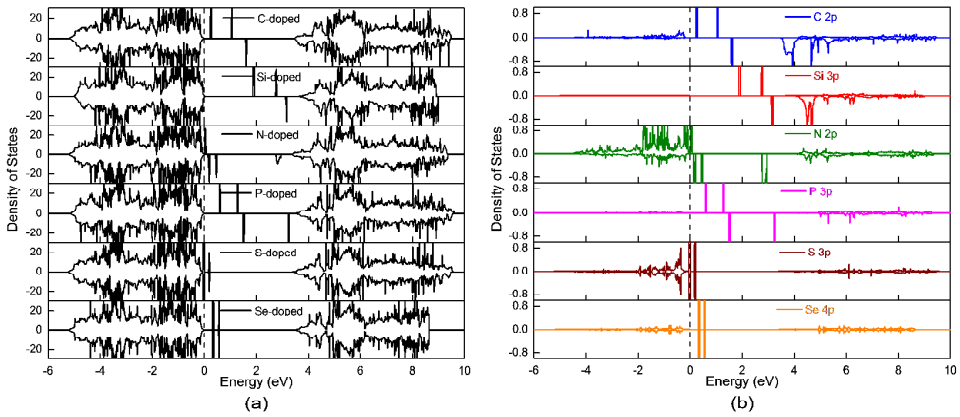

Fig. 4

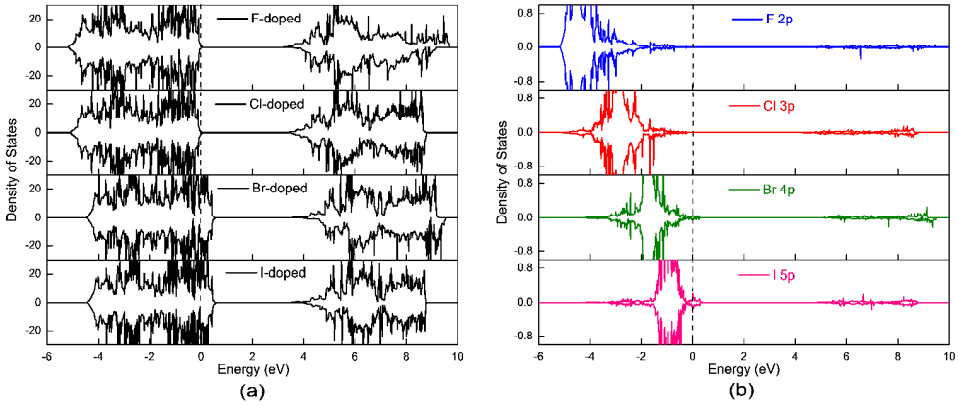

Fig. 5

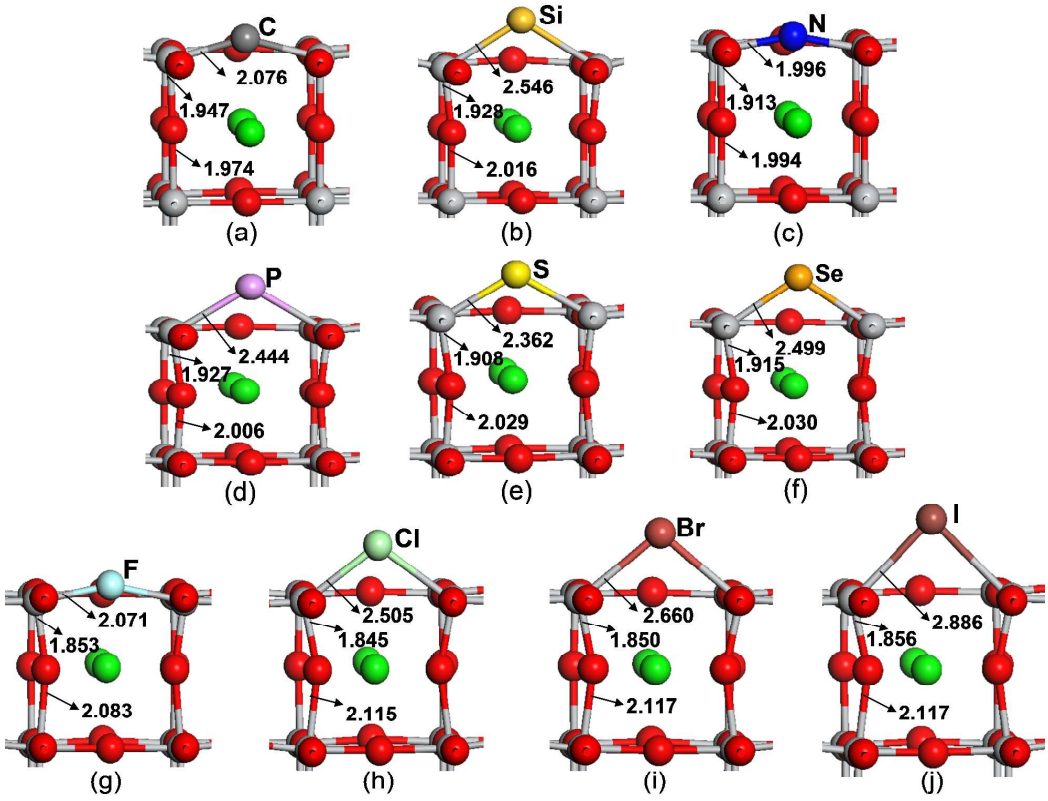

Fig. 6

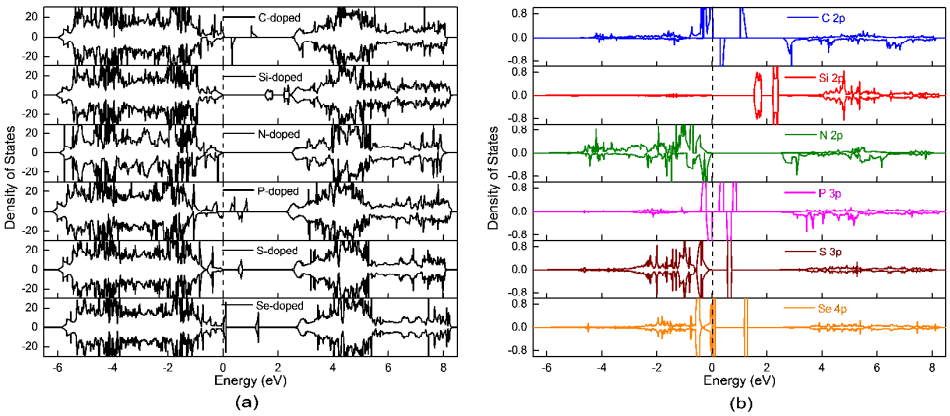

Fig. 7

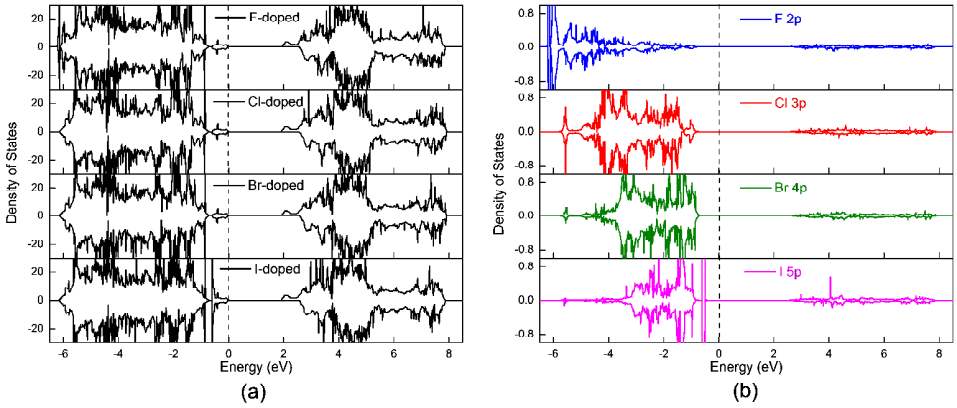

Fig. 8

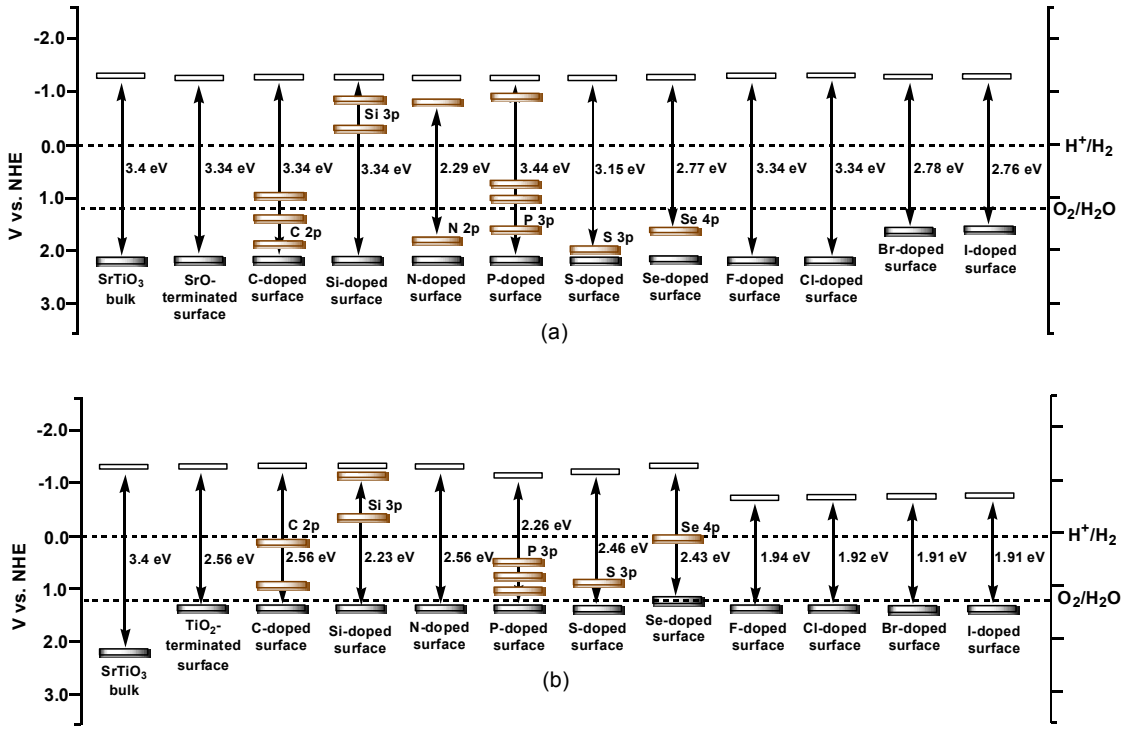

Fig. 9